Chemical Engineering Journal 150 (2009) 69–82

Contents lists available at ScienceDirect

Chemical Engineering Journal

journal homepage: www.elsevier.com/locate/cej

Choice of urea-spray models in CFD simulations of urea-SCR systems

Henrik Ström, Andreas Lundström, Bengt Andersson*

Competence Centre for Catalysis/Chemical Reaction Engineering, Chalmers University of Technology, SE-412 96 Göteborg, Sweden

ARTICLE INFO

Article history:
Received 18 June 2008
Received in revised form 2 December 2008
Accepted 3 December 2008

Keywords:
Urea spray
CFD
Lagrangian
Urea decomposition
Mass transfer
Heat transfer

ABSTRACT

The sensitivity of modeling choices to obtained results for Eulerian–Lagrangian CFD simulations of urea-SCR systems has been investigated for a system consisting of an AdBlue-spray located at the exhaust pipe wall, directed into the exhaust gas flow. The decomposition of urea is modeled as being heat transfer limited and taking place at a constant temperature (425 K). It is shown that modeling choices may affect the predicted extent of wall hit, which types of droplets that are predicted to hit the wall, and also where they will do so.

The influence of the different forces due to drag, buoyancy, lift effects, thermophoresis and history effects was investigated, proving that only the forces due to drag and buoyancy are necessary to correctly describe droplet motion within this system. It is necessary to use a droplet drag coefficient that takes the current level of droplet distortion into account.

A stochastic particle tracking model will describe the effects of turbulent dispersion, but also make the simulation results sensitive to the quality of the turbulence model's prediction of the turbulent fluctuating velocities. Using such a model will also resolve some of the enhancement of heat and mass transfer caused by the continuous acceleration/deceleration of droplets by turbulent eddies.

1. Introduction

The increasing demand on the automotive industry to reduce emissions from diesel engines entails more knowledge about the modeling of exhaust gas after treatment systems. One of the major pollutants in diesel exhaust is nitric oxides (NO_x). NO_x has adverse effects on both human health and the environment.

A promising technique for reducing NO_x emissions is selective catalytic reduction (SCR) with urea. With this approach, a water–urea solution is sprayed into the exhaust pipe in front of the catalyst. Urea will decompose into ammonia, which is the reducing agent needed to transform NO_x to N_2 on the catalyst.

Computational fluid dynamics (CFD) simulations will most probably play a crucial role in the design and optimization of future urea-SCR systems. The work presented here has investigated droplet–flow interactions in a urea-SCR-spray originating from nozzle located at the exhaust pipe wall, using commercial CFD software (Fluent 6.3.26). The main body of this work is devoted to determining the most suitable and least complex models for Eulerian–Lagrangian CFD simulations of urea-SCR systems, and to critically assess the actual impact of choosing a specific model on all studied results.

In order to identify the main characteristics of the urea-SCR system from a modeling perspective and – equally important – identify what that is too poorly known to be accurately modeled, a short description of the chemistry and physics of the urea-SCR system is necessary, and will follow below.

1.1. Urea decomposition

In the urea-SCR system, a solution of 32.5 wt% urea in water (AdBlue) is sprayed into the pipe ahead of the SCR catalyst. Water is evaporated and the resulting solid urea melts and starts to decompose thermally [1]:

$$NH_2\text{–}CO\text{–}NH_2(s) \rightarrow NH_3(g) + HNCO(g), \quad \Delta H = 185.5\,\text{kJ/mol} \tag{1}$$

This results in release of gaseous ammonia that can take part in the SCR reactions. The resulting isocyanic acid will also produce ammonia, through hydrolyzation on the SCR catalyst (or in the gas phase at high temperatures) [1]:

$$HNCO(g) + H_2O(g) \rightarrow NH_3(g) + CO_2(g) \tag{2}$$

This reaction, being limited mainly by external and internal mass transfer [2], is much faster than the SCR reactions, which means that it is believed that every mole of urea will result in two moles of ammonia for the SCR reactions.

* Corresponding author. Tel.: +46 31 772 30 26; fax: +46 31 772 30 35.
E-mail address: bengt.andersson@chalmers.se (B. Andersson).

1385-8947/$ – see front matter © 2008 Elsevier B.V. All rights reserved.
doi:10.1016/j.cej.2008.12.003

Nomenclature

Latin letters

B_M	mass transfer number
B_T	heat transfer number
C_b	TAB model constant
C_B	history force coefficient
C_D	drag coefficient
C_d	TAB model constant
C_F	TAB model constant
C_k	TAB model constant
C_L	lift coefficient
C_m	constant in the expression for the thermophoretic force
C_s	constant in the expression for the thermophoretic force
C_t	constant in the expression for the thermophoretic force
c_p	specific heat (J/kg K)
D	pipe diameter (m)
D_{AB}	diffusion coefficient of vapor in the bulk (m^2/s)
$\bar{d}$	Rosin–Rammler diameter (m)
d	diameter (m)
F	force (N)
F	force vector (N)
F_M	film thickness correction factor
F_T	film thickness correction factor
g	gravitational acceleration (m/s^2)
h	heat transfer coefficient (W/K)
ΔH	enthalpy change depending on subscript: heat of sublimation, reaction, decomposition or vaporization (J/kg)
I	turbulence intensity
k	thermal conductivity (W/m K)
k	turbulent kinetic energy (m^2/s^2)
K	spray/wall-interaction model parameter
K_0	constant for determination of the lift coefficient
K_1	constant for determination of the lift coefficient
k_c	mass transfer coefficient (m/s)
m	mass (kg)
M	molar mass (moles/kg)
n	Rosin–Rammler exponent
P	total pressure (Pa)
p	partial pressure (Pa)
r	undisturbed droplet radius (in the TAB model) (m)
R	universal gas constant (J/kg mol)
t	time (s)
T^*	spray/wall-interaction model parameter
T	temperature (K)
$\partial T/\partial x$	gas phase temperature spatial gradient (K/m)
u'	instantaneous (turbulent) velocity fluctuation (m/s)
$\bar{u}$	resolved (mean) velocity (m/s)
u	velocity (m/s)
u	velocity vector (m/s)
U_c	relative velocity between droplet and gas on the streamline through the centre of the droplet (m/s)
$\partial U/\partial y$	velocity gradient over droplet that is perpendicular to direction of droplet motion (1/s)
Y	mole fraction
y	normalized droplet distortion

Greek letters

Φ	material property
α^*	dimensionless shear rate
ϕ	factor in iterative calculation of B_T
λ	mean free path of the gas (m)
κ	ratio between particle and fluid viscosities
μ	molecular viscosity (kg m/s^2)
ρ	density (kg/m^3)
σ	surface tension between droplet and gas (N/m)
τ	integration variable
ξ	uniformly distributed random number
ζ	normally distributed random number

Superscripts and subscripts

°	saturation
AdBlue	AdBlue
c	corrected
f	film composition
film	film
g	gas
H_2O	water vapor
i	coordinate direction ($i = x, y, z$)
p	particle (droplet)
r	relative
ref	film (reference) temperature
s	surface
sat	saturation
urea	urea
vap	vapor
w	wall
wall-normal	wall-normal direction
x	subscript for identification of forces acting on droplets D = drag, B = buoyancy, L = lift, T = thermophoresis, H = history
0	initial

Dimensionless numbers

Kn	Knudsen number, $2\lambda/d_p$
Nu	Nusselt number, hd_p/k_g
Pr	Prandtl number, $c_{p,g}\mu_g/k_g$
Re	Reynolds number, $\rho_g D u_g/\mu_g$
Re_p	droplet Reynolds number, $\rho_g d_p U_c/\mu_g$
Sc	Schmidt number, $\mu_g/\rho_g D_{AB}$
Sh	Sherwood number, $k_c d_p/D_{AB}$
We	Weber number, $\rho_g d_p U_c^2/\sigma$

It has been proposed that, since urea ideally decomposes into ammonia, ammonia will be the active reducing agent [1], and thus the SCR reactions for the urea-SCR system will be the same as for an NH_3-SCR system.

1.2. Uncertainties in the urea decomposition process

When the water has more or less fully evaporated from the AdBlue droplet, it is not yet completely known what the droplet looks like. The various suggestions in the literature include a particle of solid urea [1–3] or molten urea [2–4] or just a very concentrated water solution of urea [5]. Urea has a melting temperature of approximately 406 K [6]. There are many suggestions in the literature for the temperature when urea starts to decompose thermally, for example: 406 K [7], 416 K [8], 425 K [9] and 433 K [10,11]. In fact, urea decomposition has been observed at low rates at temperatures as low as 353 K [12]. In previous studies, urea decomposition has been modeled (in order of decreasing complexity) either as evaporation with a saturation pressure curve determined from experimental data [13], with an Arrhenius expression [7,14],

as controlled by the turbulent mixing process [3], or simply with a conversion efficiency factor determined from experimental data [2]. The Arrhenius expression approach has resulted in urea decomposition modeled as taking place at temperatures as high as above 600 K [14]. For the modeling in this work, given the above-presented background, it was decided to model urea decomposition as a heat transfer limited process at a constant temperature of 425 K. This approach evades the need for empirical parameters that need to be trimmed to experimental data from a specific system.

The conversion efficiency of urea into ammonia changes with temperature. This is believed to be caused by the fact that urea decomposes in at least two stages [7]. The first stage, which is the one starting somewhere above 406 K, results in the formation of isocyanic acid and ammonia. Further heating will cause polymerization into biuret (from 433 K) and cyanuric acid and ammelide (from 448 K) [9]. The second stage starts at 523 K, where decomposition into ammonia and isocyanic acid stops. Urea may thereafter form cyanurates, ammeline, ammelide and melamine [9]. Ammonia can even be consumed during these transitions [15]. For these reasons, urea should ideally decompose at temperatures close to the start of the first stage of decomposition, in order to gain maximum urea conversion efficiency into ammonia. It is also of interest to notice that contact with the catalyst is reported to speed up the first stage, so that there will be almost no decomposition of urea at temperatures of 523 K and above [15].

Even if the thermal decomposition of urea starts already in the exhaust pipe just after injection, it will most probably not be complete by the time it reaches the catalyst entrance. Depending on the temperature of the exhaust gases, as little as 20% conversion of reaction (1) can be expected (at 330 °C), while isocyanic acid is stable enough in the gas phase to remain totally unreacted until reaching the catalyst surface [16]. In one study, no more than 65% of the injected urea had decomposed before the catalyst entrance at a flue gas temperature of 440 °C and a residence time in the exhaust pipe of 90 ms [1]. As urea decomposition only liberates half of the total molar amount of ammonia, the maximum total conversion efficiency prior to the catalyst is theoretically 50% (unless there is substantial hydrolyzation in the gas phase); this has also been supported by experimental observations [2].

1.3. Wall wetting

Deposits in the exhaust pipe in front of the catalyst have been observed in many urea-SCR systems [1,17], and the formation of melamine could be one major explanation for this [15]. It is generally believed that deposit formation is the result of a poorly adjusted AdBlue-spray [1,18]. However, it is still unclear what happens if and when the spray hits the walls, and this has been addressed only recently [13]. Depending on temperatures and droplet deformation, the effects may range from film formation (which could lead either to finalized decomposition and hydrolyzation or to deposit formation) to splashing. Today, CFD softwares often include wall-film models that can be used to predict the interaction between a spray and a wall, but these could produce ambiguous results if not all aspects of the complex pathways of urea decomposition are taken into account. Hence, the work presented here is only directed towards estimating the extent of wall hit and to clarify the underlying reasons.

2. Modeling

2.1. The system

Since the aim of the current work has been to study the influence of different modeling choices for CFD simulations of urea-SCR systems, it was decided to use a very simple and basic system setup, so as to not overshadow the implications of the choices made by the effects of an unnecessarily complex system design.

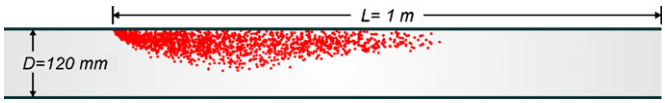

Fig. 1. Illustration of the modeled urea-SCR system.

The system simulated in this work is depicted in Fig. 1. It is a straight exhaust gas pipe with a diameter of 120 mm. A single-phase (i.e. not air-assisted) AdBlue-injector is situated at the pipe wall, directed into the flow at 45° angle. It is a pulsating injection, forming a hollow cone spray (mean half cone angle is 10°), and the distance between the injection point and the pipe outlet is 1 m. Droplets injected into the system had a number-average diameter of 93 μm and were sampled from a Rosin–Rammler diameter distribution:

$$d_p = \bar{d}(-\ln[1-\xi])^{1/n} \quad (3)$$

using random numbers ξ and with $\bar{d} = 100\,\mu m$ and $n = 1.21$. The droplet size distribution in a real-world urea-SCR system is heavily dependent on the injection system. Smaller droplets could be created by using an air-assisted injection device, for example. Although smaller droplets are generally favorable from a decomposition efficiency perspective, the use of a realistic droplet size distribution which also produces some larger droplets will allow for the inspection of the faith of both smaller and larger droplets; this approach thus gives information on the larger droplets from a single-phase injection as well as all smaller sizes of droplets (as all droplets evaporate and decompose and eventually vanish). The aim of the study is thus not to find an optimal droplet size distribution, but rather to study all occurring droplet sizes in existing urea-SCR applications. The flow rate of the injection was 2.5 g/s and the simulations each track the entire faith of one spray pulse of 10 ms. All droplets are injected with the same velocity (17.75 m/s). 10,000 computational parcels were used to represent the droplets in the spray.

Two different gas flows are considered; a typical "high" gas flow and a typical "low" gas flow. Their respective properties are summarized in Table 1. The gas is modeled as a mixture of nitrogen (75%), oxygen (10%), carbon dioxide (10%) and water (5%). The gas inlet boundary conditions are those for fully developed turbulent flow. The pressure is set to 1 atm at the pipe outlet.

To facilitate referencing to the different simulation results in this article, they are summarized and numbered in Table 2.

2.2. Eulerian–Lagrangian modeling

The most straightforward approach when doing CFD simulations of the urea-SCR system is to do it in the Eulerian–Lagrangian framework, which allows for detailed descriptions of individual droplet fates and interactions with the continuous phase.

Table 1
Properties of the "high" and "low" gas flows used in the simulations. All properties are calculated using weight-averaged mean values.

Flow property	"Low" gas flow	"High" gas flow	"Extreme" gas flow
Linear gas velocity (m/s)	25	75	100
Temperature (°C)	300	400	500
Reynolds number	~64,000	~150,000	~158,000
Streamwise turbulent intensity (%)	6.4%	5.8%	5.8%
Integral length scale (mm)	4.8	4.8	1.3
Taylor microscale (mm)	2.7	1.9	0.95
Kolmogorov length scale (μm)	150	84	57

Table 2
List of performed Eulerian–Lagrangian CFD simulations.

Case name	Case description
Case 1	High gas flow base case
Case 2	High gas flow case with detailed drag law
Case 3	High gas flow case with turbulent dispersion model
Case 4	High gas flow case with detailed drag law and turbulent dispersion model
Case 5	Low gas flow base case
Case 6	Low gas flow case with detailed drag law
Case 7	Low gas flow case with turbulent dispersion model
Case 8	Low gas flow case with detailed drag law and turbulent dispersion model
Case 9	Extreme gas flow base case
Case 10	Extreme gas flow with detailed drag law
Case 11	Extreme gas flow with turbulent dispersion model
Case 12	Extreme gas flow with detailed drag law and turbulent dispersion model

Table 3
The most commonly encountered forces in the Eulerian–Lagrangian modeling approach.

Force	Due to
Drag force	Relative velocity between droplet and gas
Buoyancy force	Gravitation
Virtual mass force	Acceleration of the surrounding gas at droplet acceleration
Brownian motion	Collisions with individual molecules of the gas phase
Lift force	Velocity gradient in the normal direction to the particle trajectory
Rotational force	Rotation of the droplet
Thermophoretic force	Temperature gradient over droplet
History force	Build-up of continuous phase boundary layer at acceleration of droplet

The gas phase flow is highly turbulent and is solved for with a two-equation turbulence model in order to provide a fast and robust simulation environment. The RNG k–ε model was chosen since it is known to better respond to the higher strain rates associated with spray-generated turbulence compared to the standard k–ε model [19], although these effects might not be large for dilute sprays, e.g. AdBlue-injections. The equations solved and the model constants and underlying assumptions are all available in full detail in [20]. RNG k–ε has been used in previous studies on exhaust gas flow [21,22]. Standard wall functions were used and the computational mesh contained approximately 168,000 hexahedral cells.

Droplet motion is then coupled to continuous phase motion via Newton's second law of motion, where the net momentum transfer between the phases can be calculated from the sum of all relevant forces acting on the droplet (Eq. (4))

$$m_p \frac{\mathrm{d}\mathbf{u}_p}{\mathrm{d}t} = \sum_x \mathbf{F}_x \tag{4}$$

This means that it is necessary to determine which forces to include in the computations *a priori* (in order to reduce complexity and time needed), based either on previous experience or sensitivity analysis.

The most commonly encountered forces are listed in Table 3. The drag force is normally the most dominating force in spray systems and should thus always be included. The buoyancy force will always be present, its influence being greater for longer retention times and heavier droplets. The virtual mass force can be safely neglected considering that the continuous phase is almost 2000 times lighter than the droplets [23]. Brownian motion becomes relevant when the size of the droplets approaches the mean free path of the continuous phase, but with the simulation setup used in the current work, droplets evaporate very fast when they reach the size where Brownian effects start to become important (approximately 1–2 μm), and Brownian motion need not be modeled [23]. If, however, such a simulation setup is not used, it is necessary to include corrections of the drag force as the droplets approach the mean free path of the gas. A suitable correction is in that case the so-called Cunningham correction [24].

The last four forces are more difficult to dismiss in advance, and have therefore been examined in more detail. They were excluded from the force balance in the simulations, but their size relative to the current drag force was logged at all times in order to verify this assumption afterwards.

2.2.1. The drag force

The drag force is calculated as

$$F_\mathrm{D} = C_\mathrm{D} \frac{\pi d_\mathrm{p}^2}{4} \frac{\rho_\mathrm{g} |U_\mathrm{c}| U_\mathrm{c}}{2} \tag{5}$$

This approach calls for a sub-model to describe the drag coefficient, C_D. Since the drag force is the most important force acting on the droplets in the spray, great care must be taken to choose a suitable model for the drag coefficient. This will therefore be discussed in detail in the following section.

2.2.2. The drag coefficient for spherical droplets

Sub-models for the droplet drag coefficient are herein referred to as *drag laws*. A common way to obtain a drag law is to use a correlation based on empirical data for the geometric shape in question. For (perfect) spheres, one such well-known equation is available in [25]:

$$C_{D,\mathrm{sphere}} = \frac{24}{Re_\mathrm{p}}(1 + 0.2\, Re_\mathrm{p}^{0.63}) \tag{6}$$

which is valid for $20 < \mathrm{Re_p} < 260$. This drag law is from here on referred to as the *spherical drag law*. The droplet Reynolds number, $\mathrm{Re_p}$, is evaluated at the free stream density and the film viscosity using the 1/3 rule (explained in Section 2.4), as this procedure has been shown to be the most accurate [26].

Different physical phenomena relating to the fluid nature of the droplet particles may necessitate corrections or alterations of the drag coefficient correlation. Such phenomena include internal circulation, droplet deformation and continuous phase turbulence.

2.2.3. The drag coefficient—effects of internal circulation

Since the surrounding fluid will exert a viscous shear on the droplet interface, internal circulation will occur to some extent. The tendency for internal circulation is governed by the viscosity ratio between the particle and the surrounding fluid:

$$\kappa = \frac{\mu_\mathrm{p}}{\mu_\mathrm{g}} \tag{7}$$

A fluid particle will have little tendency for internal circulation due to a high κ value or surface contaminants [25,27]. Internal circulation can reduce the drag coefficient to 1/3 of the corresponding drag coefficient of a solid particle with the same radius and Reynolds number [28]. Small impurities induce surface tension gradients that hinder the internal circulation and give drag coefficients reminiscent of those for solid particles.

To evaluate if AdBlue droplets will experience an effect of internal circulation which might alter their drag coefficient, the following expression was used to estimate the deviation in drag force from that of a solid sphere [27]:

$$\frac{F_{\mathrm{drag,\,with\,internal\,circulation}}}{F_{\mathrm{drag,\,solid\,sphere}}} = \left(\frac{2 + 3\,\mu_\mathrm{p}/\mu_\mathrm{g}}{3 + 3\mu_\mathrm{p}/\mu_\mathrm{g}}\right) \times \left(1 - 0.03\left(\frac{\mu_\mathrm{g}}{\mu_\mathrm{p}}\right) Re_\mathrm{p}^{0.65}\right) \tag{8}$$

This was done for AdBlue droplets in the gas flow temperatures listed in Table 1. Since the exhaust gas temperature variation will lie mainly within these ranges, and droplet viscosity will tend to increase when water is evaporated but decrease as temperature increases, κ will vary accordingly. Because of the rapid heating of injected droplets the viscosity ratio will start to decrease and pass trough a minimum value of 30 and then increase to above 95 due to the effects of water evaporation.

Three free stream velocities were examined (20, 50, 70, and 100 m/s) for six different initial droplet sizes (25, 75, 100, 150, 200, and 300 μm). The maximum deviation from a solid sphere was found to be within 5% for the largest free stream velocity and the largest droplet size at the highest temperature. However, this deviation is only seen at the beginning of the droplet lifetime and is very short-lived. Also, for a typical AdBlue-spray the droplets will be of a much smaller size than 300 μm. This shows that the effect of internal circulation is of minor importance when predicting drag for the urea-SCR system. It is therefore neglected in the current work.

2.2.4. The drag coefficient—effects of droplet deformation

Deformation of droplets is another phenomenon that will affect the drag coefficient. Droplets remain spherical as long as surface tension and/or viscous forces are much larger than the inertial forces exerted by the surrounding fluid. For high Reynolds numbers ($Re_p > 600$) almost all droplets will deform [25]. Droplets will experience greater drag if their shapes are distorted (up to 2 or 3 times greater), although for the lower range of particle Reynolds numbers ($Re_p < 1000$) this effect is not always as pronounced [28].

If a measure of the droplet distortion is available, it is possible to calculate the drag coefficient as a simple linear variation between the spherical drag coefficient and the constant 1.54 (which corresponds to the drag coefficient of a disk at the prevailing particle Reynolds numbers [20], and also has been found to be an approximate value for fragmenting drops in incompressible flow [28]), as a function of the normalized droplet distortion, y:

$$C_{D,\text{dynamic}} = (C_{D,\text{disk}} - C_{D,\text{sphere}})y + C_{D,\text{sphere}} \tag{9}$$

Note that this drag law needs yet another sub-model to supply the current level of droplet distortion. The Taylor analogy breakup (TAB) model can help estimate the normalized droplet distortion by solving the following equation, based on the analogy between an oscillating droplet and a spring-mass system [20]:

$$\frac{d^2y}{dt^2} = \frac{C_F}{C_b}\frac{\rho_g}{\rho_p}\frac{U_c^2}{r^2} - \frac{C_k\sigma}{\rho_p r^3}y - \frac{C_d\mu_p}{\rho_p r^2}\frac{dy}{dt} \tag{10}$$

A value of $y = 0$ corresponds to an undisturbed droplet, whereas $y = 1$ means the droplet distortion is equal to half of the undisturbed droplet radius, which would make the droplet look like a disc. The approach of using the TAB model to vary the drag coefficient was originally introduced into the KIVA CFD code [22]. One important difference between this approach and regular correlations is that it supplies time resolved values for the droplet drag coefficient, thus also capturing effects of droplet viscosity on the deformation process. It could be speculated that this additional historical information may be important for transient behavior of the droplets. However, the spring-mass analogy on which the TAB model is based limits the reliability of these time resolved effects, as it implies restrictions on the oscillation mode undertaken by the droplet and is of course dependent on the initial deformation specified.

Another drag coefficient is reported in [29] which accounts for droplet oscillation/deformation as well as effects of evaporation (the so-called "blowing" effect [30]). The correlation in [29] does not account for droplet internal circulation, since only contaminated systems and high kappa ratios were considered. In [27], both the change of droplet shape/aspect ratio and internal circulation was taken into account, but effects of evaporation were not considered.

When adjusting the correlation from [29] for internal circulation, it has been shown that this correlation over-predicts the sensitivity to the Weber number in the small Reynolds number range ($Re_p < 20$) [27]. For the $20 < Re_p < 200$ range, good agreement with computational results was found [27]. This range includes the most representative particle Reynolds numbers for a urea-SCR system (in the limit of the largest droplets in the system, Re_p may be as high as ~300).

One possibility could be to use the correlation from [29] and adjust it for internal circulation using the procedure developed in [27]. However, since the range of simulation conditions used in [27] seems to lie well outside the range for the urea-SCR system, we choose not to speculated whether such an approach would be beneficial or not.

The correlation examined in this work for the urea-SCR system is thus the one suggested in [29]:

$$C_D = C_{D,\text{sphere}}(1 + B_T)^{-0.2}(1 + 0.06Re_p^{-0.12}\,\text{We}^{1.4}) \tag{11}$$

It uses the drag coefficient of a sphere (as calculated by Eq. (6)) and adjusts it for evaporation (via the heat transfer number, B_T; further discussed in Section 2.4) and droplet deformation (via the particle Reynolds number and the Weber number, We). Once all water has left the droplet and pure solid urea is left, the droplet is assumed not to distort and the correction for droplet deformation is dropped (i.e. the droplet is treated as a perfect evaporating sphere from this point on). This drag law is from here on referred to as the *detailed drag law*. The assumption of a non-distorting urea droplet is justified by the fact that the relative velocity between the droplet and the gas will be small at the start of urea decomposition, in combination with the high viscosity of the urea melt, which will effectively slow down any incipient droplet deformation.

It should be noted that the correlation above was developed for evaporating droplets of *n*-heptane and not AdBlue. However, experiments have shown that the reduction in drag is very similar between evaporating droplets of water and heptane at the current Reynolds numbers [26]. The droplet Reynolds number is still evaluated at the free stream density and the film viscosity [29,26].

2.2.5. The drag coefficient—effects of continuous phase turbulence

Lastly, also the effects of gas phase turbulence on droplet drag coefficient may be taken into account. On smaller scales, comparable with the droplet size (typically on the Kolmogorov scale), the effects of turbulence may be seen as an increase in drag coefficient. Usually the drag coefficient increases with increasing relative intensity (i.e. fluctuating velocity over particle relative velocity) [31]. Increasing drag coefficients for increasing relative intensity measured for rigid spheres in liquids was reported in [32]. These results were however not deemed applicable for sprays due to experiments being conducted at low-density ratios ρ_p/ρ and spatial scales of turbulence not comparable to those found in a typical combustion spray [31]. Later, Anderson and Uhlherr [33] attributed the increase in drag with relative intensity to the previous method used in [32] for computing the relative velocity between the dispersed and continuous phase. For low intensities (<10%), the drag coefficient was found to decrease [34]. In [31], drag coefficients applicable for spray conditions are calculated from average drag forces over a displacement using three measurement locations. However, no conclusive and systematic deviation from the drag-coefficient correlation given by [25] can be noticed. Because of the uncertainties in the correlations for the effects of continuous phase turbulence on particle drag coefficients, this effect has not been considered in the current work.

2.2.6. The buoyancy force

The buoyancy force is modeled as

$$F_{B,i} = m_p \frac{g_i(\rho_p - \rho_g)}{\rho_p} \tag{12}$$

The buoyancy force is expected to be second largest force after the drag force. However, since the injector is situated at the wall in the investigated injection system, inclusion of the buoyancy force would create an innumerable set of system setups—since the position of the injector relative to the gravity vector will influence the simulation results. It was therefore decided to remove the buoyancy force from the computations and instead only estimate its influence in terms of droplet displacement.

In the simulations performed, the droplet retention times in the pipe ranges approximately from 20 to 40 ms. This translates to a displacement of the droplets by the buoyancy force that is in the range 1–7% of the pipe diameter. It is evident that neglecting the buoyancy force has little effect for the shortest retention times, whereas for the longer retention times the predicted results will be influenced. Neglecting the buoyancy force can be justified based on the very purpose of the current investigation, but this force should otherwise always be included in simulations of AdBlue-sprays.

2.2.7. The lift force

A droplet moving parallel to a velocity gradient will experience a lift force often referred to as the Saffman lift force. For the AdBlue-spray droplets, it is obligated to use an expression that can handle high particle Reynolds numbers ($Re_p \gg 1$). One such expression is presented in [35].

In order to investigate whether the lift force should in fact be included in the Lagrangian force balance during simulations of an AdBlue-spray, all simulation cases 1–12 were performed with an ad hoc routine that logged the size of the lift force of all droplets at all times. The lift force was calculated from:

$$F_L = \frac{1}{8} C_L \rho_g U_c^2 \pi d_p^2 \tag{13}$$

A simplified version of the expression suggested by Kurose and Komori was used for the lift coefficient C_L [35] (the simplification being that the droplet is assumed not to rotate):

$$C_L(Re_p, \alpha^*) = K_0 \alpha^{*0.9} + K_1 \alpha^{*1.1} \tag{14}$$

where K_0 and K_1 are constants linearly interpolated from Table 3 in [35], and α^* is the dimensionless shear rate of the fluid. The expression (13) is valid for $1 \le Re_p \le 500$ and $0 \le \alpha^* \le 0.4$, and the dimensionless shear rate is defined as

$$\alpha^* = \frac{1}{2} \frac{d_p}{U_c} \frac{\partial U}{\partial y} \tag{15}$$

To simplify the code in order to speed up the computations, the velocity gradient $\partial U/\partial y$ was taken as the *largest* velocity gradient over the droplet in any direction, rather than the actual velocity gradient in the plane perpendicular to the droplet motion direction, as in the definition of the lift force. This leads to an estimation of the dimensionless shear rate that is always equal to or *larger* than what is actually experienced by the droplet, and thus most probably an *overestimation* of the current lift force.

2.2.8. The rotational force

Droplet rotation produces a lift force known as the Magnus lift force. The direction of this force is dependent on the direction of droplet rotation relative to the gas flow. Resolving rotational effects necessitates the solving of one more equation per computational parcel (for the rotational speed) and is thus computationally expensive. It has been shown that rotational effects can be expected to be unimportant if lift force effects also are negligible, as the lift force by rotation is often less by an order of magnitude than that due to shear [36].

2.2.9. The thermophoretic force

Temperature gradients are known to exist in the pipe at the point of evaporation and decomposition of the spray, so thermophoresis (the force on a particle due to a temperature gradient) is a potentially important effect. In order to investigate whether the thermophoretic force should be included in the force balance during simulations of an AdBlue-spray, all simulation cases 1–12 were performed with an ad hoc routine that logged the size of the thermophoretic force for all droplets at all times. The expression used to calculate the thermophoretic force was taken from Talbot et al. [37]:

$$F_T = -\frac{6\pi d_p \mu_g^2 C_s((3.75\mu_g R/k_p) + C_t Kn)}{\rho_g(1 + 3C_m Kn)(1 + (7.5\mu_g R/k_p) + 2C_t Kn)} \frac{1}{T_g} \frac{\partial T_g}{\partial x} \tag{16}$$

The gas phase temperature gradient over the particle was always taken to be the largest present gradient, so as to always obtain the magnitude of the largest thermophoretic force.

2.2.10. The history force

The history force (sometimes known as the Basset force) is the force arising from the build-up and/or rearrangement of the boundary layer around the droplet at acceleration/deceleration. It is only important at very short times during acceleration of the particle in large velocity gradients [23], and its importance decreases with increasing particle density and/or increasing particle size.

It is, as previously stated, necessary to use an expression that is valid for high particle Reynolds numbers. The influence of history effects between times t_{p0} and t_p was therefore estimated using the expression in [38]:

$$F_H = \frac{3}{2} d_p^2 \sqrt{\pi \rho_g \mu_g} \cdot C_B \cdot \int_{t_{p0}}^{t_p} \frac{(\mathrm{d}/\mathrm{d}\tau)(\mathbf{u}_g - \mathbf{u}_p)}{\sqrt{t_p - \tau}} \, \mathrm{d}\tau \tag{17}$$

with

$$C_B = 0.48 + \frac{0.52}{((|u_g - u_p|^2)/(d_p|(\mathrm{d}/\mathrm{d}t)(\mathbf{u}_g - \mathbf{u}_p)|) + 1)^3} \tag{18}$$

Assuming a linear change in relative velocity, the size of the history force relative to the current drag force could be calculated *a posteriori* for all time steps of all performed simulation cases. Since this means that the history force is not solved for explicitly, this approach will only provide an *approximation* of the magnitude of the history force.

2.3. Turbulent effects on droplet trajectories

Another prioritized area of interest in the present work has been to investigate the sensitivity of the simulation results to whether stochastic tracking of droplets was used or not. To estimate the importance of turbulence on particle drag, it is possible to calculate the relative turbulence intensity, I_r [30]:

$$I_r = \frac{\sqrt{\langle u'^2 \rangle}}{|\langle u \rangle - u_p|} \tag{19}$$

It is obvious that I_r is augmented as the droplet is accelerated by the gas flow, and therefore turbulence effects will be large so as to require modeling in the urea-SCR system. Stochastic tracking is one way to take into account the effect of turbulent eddies interacting with the droplets. A popular model is known as the Discrete Random Walk (DRW) model. In the DRW model, eddies are characterized by a pseudo-random velocity fluctuation and a time scale.

During the integration of the trajectory equations for the individual droplets, the gas phase velocity is taken as the sum of the mean (resolved) part and an instantaneous velocity fluctuation:

$$u = \bar{u} + \zeta\sqrt{\langle u'^2\rangle} \tag{20}$$

Here, ζ is a normally distributed random number, as it is assumed that the velocity fluctuation obeys a Gaussian distribution. For the k–ε models the fluctuating component $\sqrt{\langle u'^2\rangle}$ is equal to $\sqrt{2k/3}$ in all coordinate directions, since they are based on the assumption of isotropic turbulence.

This piecewise constant velocity fluctuation of the gas phase is assumed to prevail for the shortest of the eddy lifetime and the time it would take for the particle to cross through the eddy. The eddy lifetime is calculated as a random variation about the fluid Lagrangian integral time. At the end of the shortest of the eddy lifetime and the particle eddy crossing time, the droplet is assumed to enter a new eddy, and the process is repeated, starting over with new random numbers in Eq. (20).

2.4. Droplet heat and mass transfer

Two-way coupling is employed for the heat and mass transfer between the continuous and dispersed phases, and dispersed phase evaporation and decomposition is simulated as a three-step process:

As a first step, water leaves the droplet through evaporation. Vaporization is assumed to be governed by gradient diffusion, where the partial pressure of water vapor at the droplet surface is assumed to be equal to the saturation pressure of water over an AdBlue solution of the current composition and temperature. In the heat balance, the sensible heat change in the droplet is related to the convective and latent heat transfer between the droplet and the gas. The heat and mass transfer coefficients are determined from Nusselt and Sherwood correlations, respectively (Eqs. (31) and (32)), which during this evaporation phase are adjusted to account for the effect of mass transfer, in accordance with the method used in [14]. The heat and mass balances thus become:

$$\frac{\mathrm{d}m_\mathrm{p}}{\mathrm{d}t} = -\pi d_\mathrm{p}\rho_{f,\mathrm{ref}}D_{AB,\mathrm{ref}}\mathrm{Sh_c}\,\ln[1+B_M] \tag{21}$$

$$\frac{\mathrm{d}T_\mathrm{p}}{\mathrm{d}t} = \frac{(-\mathrm{d}m_\mathrm{p}/\mathrm{d}t)c_{\mathrm{p,vap,ref}}(T_\mathrm{g}-T_\mathrm{p})/B_T - \Delta H_\mathrm{vap}}{m_\mathrm{p}c_{\mathrm{p,AdBlue}}} \tag{22}$$

where B_M is the mass transfer number and B_T the heat transfer number, as defined by:

$$B_M = \frac{Y_{\mathrm{vap,s}} - Y_{\mathrm{vap,g}}}{1 - Y_{\mathrm{vap,s}}} \tag{23}$$

$$B_T = (1+B_M)^{\phi} - 1 \tag{24}$$

The dimensionless surface concentration of water vapor is

$$Y_{\mathrm{vap,s}} = \frac{p^{\circ}_{\mathrm{H_2O}}}{P} \tag{25}$$

whereas $Y_{\mathrm{vap,g}}$ is the gas bulk concentration.

Since

$$\phi = \frac{c_{\mathrm{p,vap,ref}}}{c_{\mathrm{p,f,ref}}}\frac{\mathrm{Sh_c}}{\mathrm{Nu_c}}\frac{Pr_{\mathrm{f,ref}}}{\mathrm{Sc_{f,ref}}} \tag{26}$$

and

$$\mathrm{Nu_c} = 2.0 + \frac{\mathrm{Nu_0} - 2.0}{F_T} \tag{27}$$

$$\mathrm{Sh_c} = 2.0 + \frac{\mathrm{Sh_0} - 2.0}{F_M} \tag{28}$$

with

$$F_T = \frac{(1+B_T)^{0.7}\log[1+B_T]}{B_T} \tag{29}$$

$$F_M = \frac{(1+B_M)^{0.7}\log[1+B_M]}{B_M} \tag{30}$$

the solution procedure is iterative for B_T.

The Nusselt and Sherwood correlations used are from Frössling [39]:

$$\mathrm{Nu_0} = 2.0 + 0.552\,Re_\mathrm{p}^{0.5}\,Pr^{1/3} \tag{31}$$

$$\mathrm{Sh_0} = 2.0 + 0.552\,Re_\mathrm{p}^{0.5}\;\mathrm{Sc}^{1/3} \tag{32}$$

where $\mathrm{Re_p}$ is evaluated at the free stream density and the film viscosity, as this has been shown to improve the predictions [40].

Material properties in the film are evaluated using the 1/3 rule [40] and the Herning and Zipperer model [41] as the mixing rule, since this model has exhibited very good performance in calculating physical properties of gas films surrounding droplets in turbulent evaporating sprays [42]:

$$T_\mathrm{film} = T_\mathrm{p} + \frac{1}{3}(T_\mathrm{g} - T_\mathrm{p}) \tag{33}$$

$$Y_\mathrm{film} = Y_{\mathrm{vap,s}} + \frac{1}{3}(Y_{\mathrm{vap,g}} - Y_{\mathrm{vap,s}}) \tag{34}$$

$$\Phi_\mathrm{film} = \frac{Y_\mathrm{film}\Phi_\mathrm{vap}}{Y_\mathrm{film} + (1-Y_\mathrm{film})(M_\mathrm{g}/M_\mathrm{vap})^{1/2}} + \frac{(1-Y_\mathrm{film})\Phi_\mathrm{g}}{Y_\mathrm{film}(M_\mathrm{vap}/M_\mathrm{g})^{1/2} + (1-Y_\mathrm{film})} \tag{35}$$

After all water is gone, the remaining part of the droplet is assumed to be pure solid urea, which is then heated to a temperature of 425 K. There is no mass exchange with the gas phase during this stage. The sensible heat change in the droplet is assumed to be equal to the convective heat transfer from the surroundings:

$$\frac{\mathrm{d}T_p}{\mathrm{d}t} = \frac{\pi d_p k_{\mathrm{g,ref}}\mathrm{Nu_0}(T_\mathrm{g} - T_\mathrm{p})}{m_\mathrm{p}c_{\mathrm{p,urea}}} \tag{36}$$

As soon as a computational parcel reaches above 425 K, urea is assumed to start to decompose, and the temperature is then held constant. Instead of a normal heat of vaporization, a fictive heat of decomposition is used, i.e. urea sublimation and decomposition are assumed to proceed in one fast step:

$$\Delta H_\mathrm{decomposition} = \Delta H_\mathrm{sublimation} + \Delta H_\mathrm{reaction} \tag{37}$$

where $\Delta H_\mathrm{sublimation}$ is the heat of sublimation of urea, and $\Delta H_\mathrm{reaction}$ is the heat of reaction for the reaction where urea decomposes into ammonia and isocyanic acid in the gas phase. The mass balance is

$$\frac{\mathrm{d}m_p}{\mathrm{d}t} = -\frac{\pi d_\mathrm{p}k_{\mathrm{g,ref}}\mathrm{Nu_0}}{c_{\mathrm{p,f,ref}}}\ln\left[1 + \frac{c_{\mathrm{p,f,ref}}(T_\mathrm{g} - T_\mathrm{p})}{\Delta H_\mathrm{decomposition}}\right] \tag{38}$$

This means that the hydrolyzation of isocyanic acid is not considered; the simulations deal only with the decomposition and mixing of the AdBlue spray in the exhaust gas flow.

A typical droplet fate is illustrated in Fig. 2.

2.5. Wall-film modeling

Since no wall-film model is used in the present study, whereas such models have been incorporated into earlier work on the urea-SCR system (for example, in [13]), it is also of interest to evaluate the possible influence of the sensitivity to the model choices presented here on the performance of a wall-film model. In [13], a wall-film

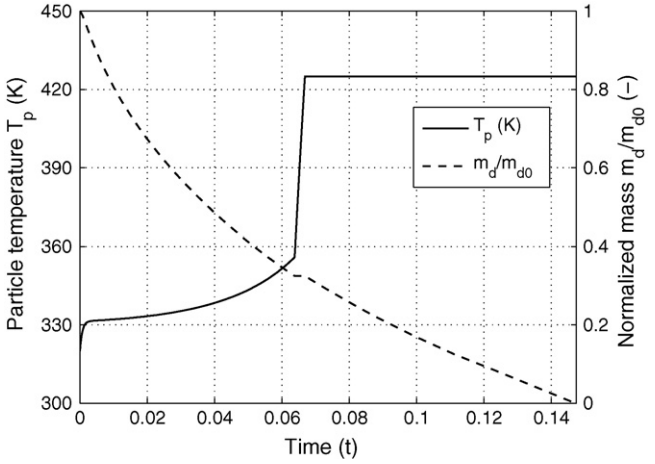

Fig. 2. Typical droplet fate.

model based on the work by Kuhnke [43] is used. The outcome of spray/wall-interaction is determined from a regime map through the use of two parameters, K and T^*:

$$K = \frac{(\rho_p d_p)^{3/4} u_{p,\text{wall-normal}}^{5/4}}{\sigma^{1/2} \mu_p^{1/4}} \tag{39}$$

$$T^* = \frac{T_w}{T_{sat}} \tag{40}$$

The highest value of T^* would correspond to a well-insulated section of the wall hitherto unaffected by any cooling effects from impacting droplets. This would correspond to 1.70 and 1.45 for the high and low gas flow simulations, respectively.[1] For these values of T^*, the parameter K would be used to differentiate between rebound and thermal breakup of droplets. However, the critical transition temperature between hot and cold wall behavior was estimated to $T^* \approx 1.4$ in [14]. It could very well be possible to reach such conditions in the present study, as it would only require a local cooling of the wall with about 20 K in the low gas flow case.

The parameter K can be calculated from our simulation data for all droplets upon collision with the wall. The two critical K numbers between rebound and thermal breakup at high T^*, and between deposition and splashing at low T^*, range within 40–45 and 130–200, respectively [43]. The balance between the numbers of droplets above and below the critical K values as a function of modeling choices will be investigated and discussed.

3. Material data

When droplets are injected and transported by the exhaust gas stream they are heated and water evaporates until only pure urea is left. During the evaporation phase droplets will contain a mixture of urea and water. Since material properties depend on both temperature and mass fraction of urea, good material data is needed to make good model predictions.

The material data used is summarized in Table 4 for the gaseous phase and Table 5 for the droplet phase. This is the – to the authors' knowledge – best existing data for the urea-SCR system. For droplet viscosity we carried out measurements of our own. AdBlue saturation pressure and density were taken from [44].

[1] The saturation temperature of AdBlue is in reality not a constant but a function of the mass fraction of urea in the droplet. For this estimation, a representative value of 395 K was used (corresponding to circa 70% urea).

Table 4
Material data for the gas phase. All material data properties are functions of temperature. The values reported in this table refer to those valid at the temperature of the flow listed in Table 1. All gas phase data was taken from [46].

Material data property	"Low" gas flow	"High" gas flow	"Extreme" gas flow
Density (kg/m^3)	0.61	0.52	0.46
Molecular viscosity (Pa s)	2.93×10^{-5}	3.23×10^{-5}	3.55×10^{-5}
Thermal conductivity (W/m K)	0.045	0.052	0.059
Specific heat (J/kg K)	1050	1069	1091

4. Results

4.1. Typical Eulerian–Lagrangian simulation results

In order to discuss changes in the simulation results due to different modeling choices, the typical results from Eulerian–Lagrangian simulations of the AdBlue-spray should first be established.

The smaller droplets will be dragged away by the main flow more quickly and will thus appear on the side of the pipe closest to the injector. Since the smallest droplets also are the ones that will lose their water and start to decompose first, most of the ammonia released ahead of the catalyst entrance will be present in this part of the pipe. These results can be seen in Figs. 3 and 4.

4.2. Sensitivity of wall hit predictions to modeling choices

A considerable number of droplets will hit the wall somewhere before they reach the pipe outlet. When discussing the wall hit results, it was found convenient to classify the droplets by where they hit the wall, and the droplet mass fraction of water at doing so. The droplets can then schematically be divided into seven groups, which are listed in Table 6.

The simulation results concerning droplet fates are presented in Fig. 5 for the high gas flow simulations, in Fig. 6 for the low gas flow simulations and in Fig. 7 for the extreme gas flow simulations. Wall hit results are specially depicted in Fig. 8.

An illustration of the extent of droplet wall impaction on the pipe walls can be found in Fig. 9 for two different simulation cases.

4.3. Sensitivity of decomposition efficiency predictions to modeling choices

The predicted decomposition efficiency, measured as the percentage of total injected mass of urea that has undergone thermal decomposition into ammonia and isocyanic acid, is presented in Table 7. The largest effect on the predicted decomposition efficiency is seen when the stochastic tracking model is turned on or off (compare cases 3–4, 7–8 and 11–12 with their respective base cases in Table 7). The order of magnitude of the decomposition efficiencies matches what has been reported in earlier studies (see Section 1.2).

Table 5
Material data for the AdBlue droplets. Numbers in brackets refer to references containing functions or data points that have been used. A star (*) implies data for pure water has been used. A diamond (♦) implies data was calculated from that of pure water at the saturation temperature and pressure of Adblue. A line (–) implies data not being used in simulations and therefore not supplied. Pure water data has been taken from [47].

Material data property	AdBlue	Urea
Density (kg/m^3)	[44]	1330.0
Thermal conductivity (W/m K)	*	–
Specific heat (J/kg K)	*	[39]
Vapor pressure (Pa)	[44]	–
Heat of vaporization (J/kg)	♦	3,095,995 (explained in Section 2.4)
Surface tension (N/m)	*	–

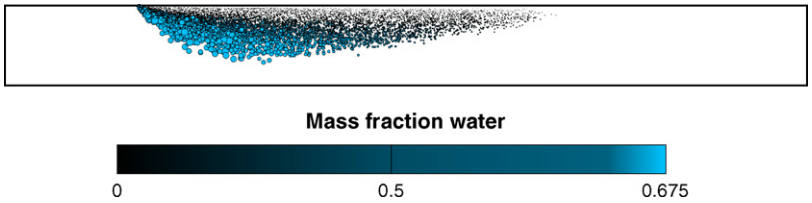

Fig. 3. Mass fraction of water in droplet. Droplet parcels are scaled by droplet diameter and magnified by a factor of 30. The parcels are colored by the mass fraction of water in the droplets. The picture is taken from the case 1 simulation and is a snapshot at 10 ms after injection.

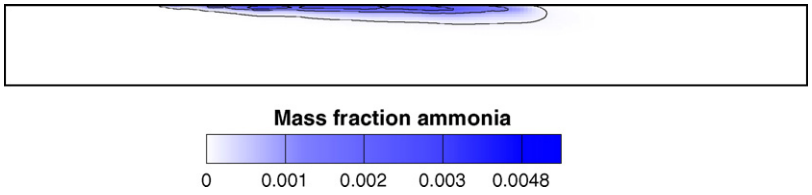

Fig. 4. Mass fraction of ammonia in pipe. The picture is taken from the same simulation and at the same time and with the same view as the picture in Fig. 3. The plane perpendicular to the main gas flow direction is colored by the mass fraction of ammonia.

Table 6
Droplet fates at wall hit.

Group	Droplet fate
i	Droplets hitting the side of the pipe wall opposite the injector, which still contain water (i.e. they are still AdBlue droplets)
ii	Droplets hitting the side of the pipe wall opposite the injector, which have lost all water and are pure urea
iii	Droplets hitting the side of the pipe wall where the injector is located, which still contain water (i.e. they are still AdBlue droplets)
iv	Droplets hitting the side of the pipe wall where the injector is located, which have lost all water and are pure urea
v	Droplets reaching the pipe outlet, which still contain water (i.e. they are still AdBlue droplets)
vi	Droplets reaching the pipe outlet, which have lost all water and are pure urea
vii	Droplets totally evaporated and decomposed within the pipe

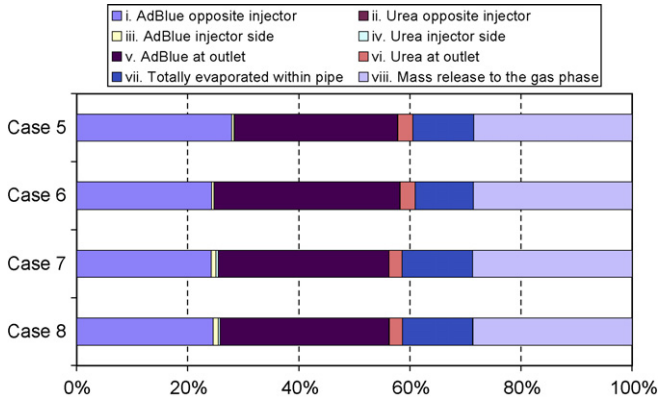

Fig. 6. Simulation results for the low gas flow simulations (cases 5–8). The different droplets fates listed in the legend at the top are presented as *percent of the total injected mass* when collected at the wall or the outlet or fully evaporated. In this context, droplet fate (vii) "Mass release to gas phase" refers to the total mass of water and urea that has left the droplets within the pipe during the simulation.

4.4. Relative sizes of neglected forces

Since the integrated transferred momentum via the (over)estimated lift force over the droplet lifetime is approximately three orders of magnitude smaller than the integrated transferred momentum via drag for all droplets in the system, neglecting the lift force is justified. This also supports the decision of neglecting the rotational force (see Section 2.2.8). These results

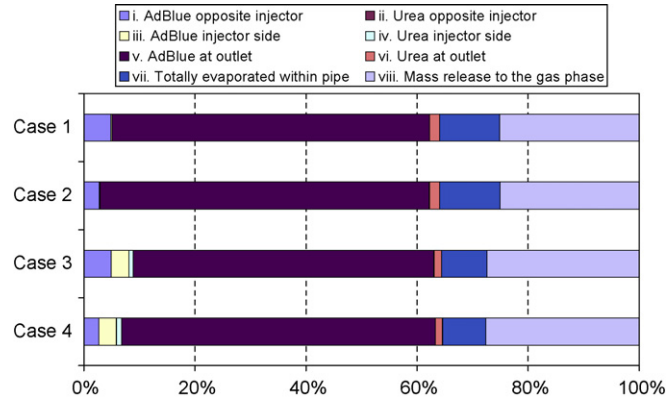

Fig. 5. Simulation results for the high gas flow simulations (cases 1–4). The different droplets fates listed in the legend at the top are presented as *percent of the total injected mass* when collected at the wall or the outlet or fully evaporated. In this context, droplet fate (vii) "Mass release to gas phase" refers to the total mass of water and urea that has left the droplets within the pipe during the simulation.

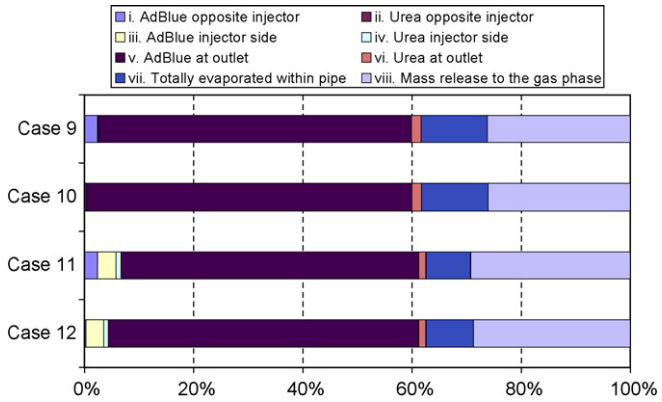

Fig. 7. Simulation results for the extreme gas flow simulations (cases 9–12). The different droplets fates listed in the legend at the top are presented as *percent of the total injected mass* when collected at the wall or the outlet or fully evaporated. In this context, droplet fate (vii) "Mass release to gas phase" refers to the total mass of water and urea that has left the droplets within the pipe during the simulation.

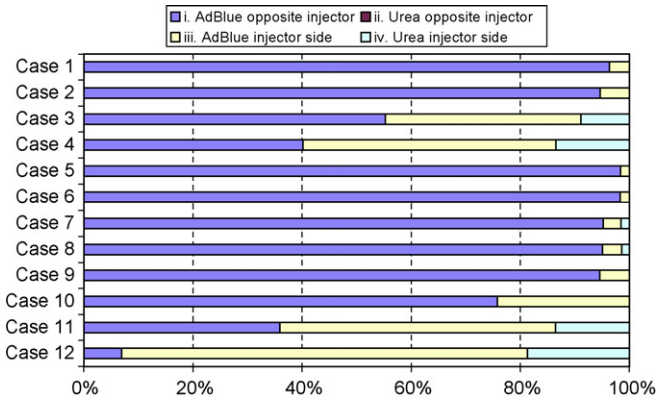

Fig. 8. Wall hit results for simulation cases 1–12. Droplets hitting walls in the simulations are classified and the four different classes are depicted as percent of the total mass of droplets with the fate in question.

Table 7
Decomposition efficiency for the high and low gas flow cases, respectively. Decomposition efficiency is defined as the percentage of total injected mass of urea that has undergone thermal decomposition into ammonia and isocyanic acid.

	Decomposition efficiency	Relative change
High gas flow cases		
Case 1 (reference case)	15.04%	
Case 2	15.05%	+0.07%
Case 3	13.12%	−12.8%
Case 4	12.82%	−14.8%
Low gas flow cases		
Case 5 (reference case)	17.01%	
Case 6	16.51%	−2.9%
Case 7	19.31%	+13.5%
Case 8	19.28%	+13.3%
Extreme gas flow cases		
Case 9 (reference case)	16.53%	
Case 10	16.59%	+0.4%
Case 11	13.84%	−16.3%
Case 12	14.23%	−13.9%

are illustrated in Fig. 10. It should however be kept in mind that the drag and lift forces are always perpendicular to each other, and trajectories may therefore still be influenced by a small lift force.

The thermophoretic force is somewhat larger at lower gas flows, but always so small that it can be neglected. It is also generally smaller than the (over)estimated lift force. These results are illustrated in Fig. 11.

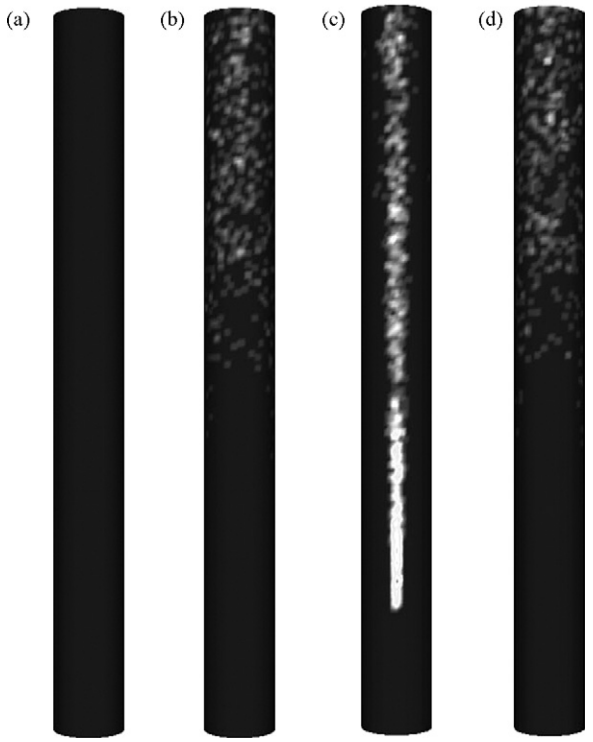

Fig. 9. Areas of droplet wall hit: (a) droplet wall hit on the injector side of the pipe for case 2; (b) droplet wall hit on opposite side for case 2; (c) droplet wall hit on the injector side of the pipe for case 4; and (d) droplet wall hit on opposite side for case 4.

History effects are sensitive to other modeling choices, most notably whether turbulent dispersion of droplets is also modeled at the same time or not. Fig. 12 illustrates how turning on the turbulent dispersion model for the droplets (cases 3–4, 7–8 and 11–12) will change the importance of history effects relative to the respective base case. History effects are also much larger than lift effects or the effects of thermophoresis, but still only a few percent of the drag force in terms of total transferred momentum. The history force will also always be acting in the same direction as the drag force.

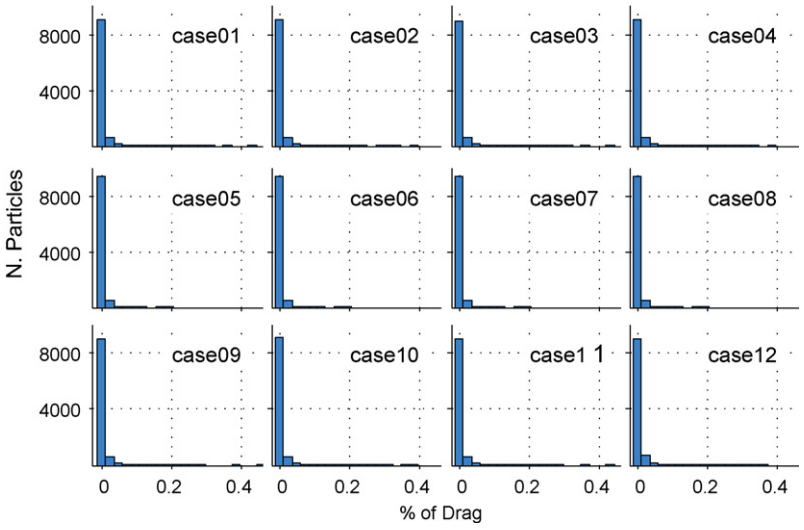

Fig. 10. Influence of the lift force relative to the drag force for simulation cases 1–12. The histograms illustrate the transferred momentum to the droplet via the lift force to that transferred via the drag force integrated over the droplet's lifetime (in percent).

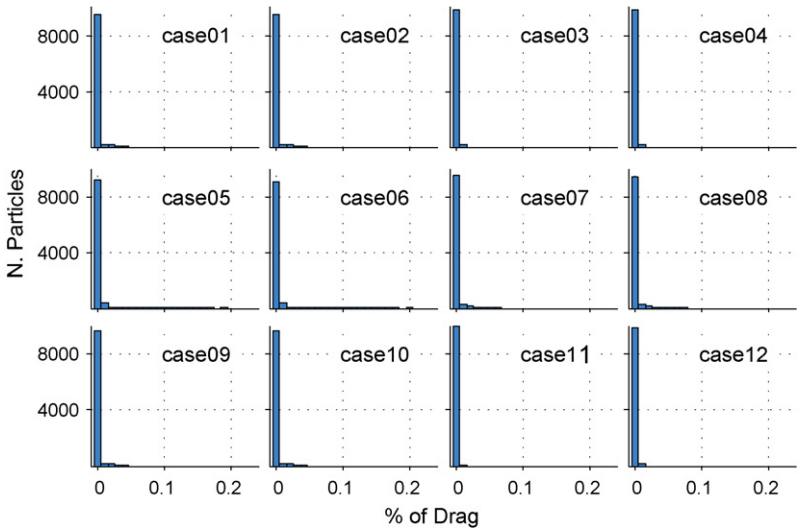

Fig. 11. Influence of the thermophoretic force relative to the drag force for simulation cases 1–12. The histograms illustrate the transferred momentum to the droplet via the thermophoretic force to that transferred via the drag force integrated over the droplet's lifetime (in percent).

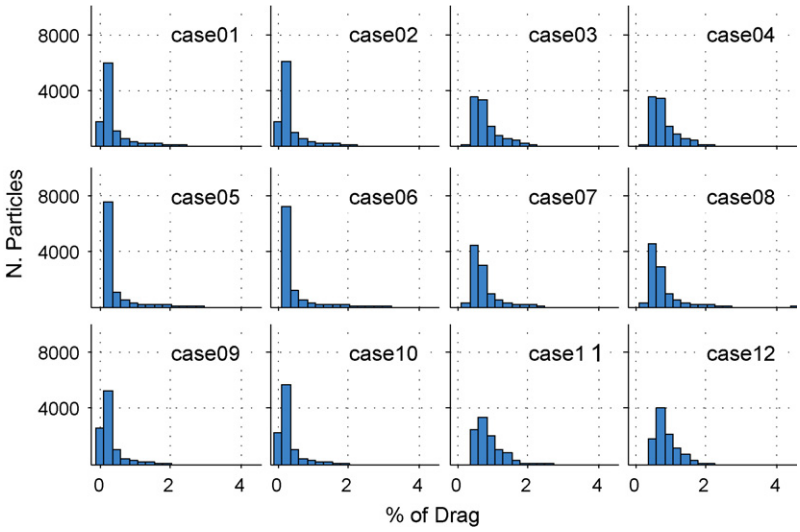

Fig. 12. Influence of the history force relative to the drag force for simulation cases 1–12. The histograms illustrate the transferred momentum to the droplet via the history force to that transferred via the drag force integrated over the droplet's lifetime (in percent).

4.5. Wall-film modeling

In Fig. 13, it is illustrated how the wall-film model parameter K is affected by the modeling choices in the gas phase. Both the total number of parcels within the different regimes of K, as well as the balance between the regimes, is changed with the different modeling choices. The pure urea particles have been omitted from this analysis.

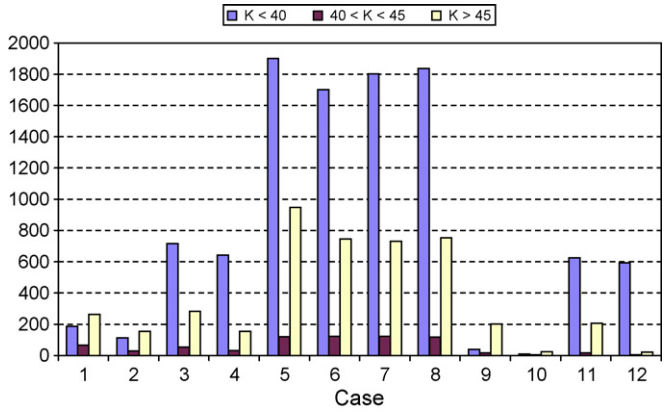

Fig. 13. Wall-film model value of parameter K for the different cases.

5. Discussion

The first and most important observation is of course that the choice of models influences the simulation results. Thus, the anticipated droplet fates in this system are also a function of the different sub-models used for the discrete phase in the performed Eulerian–Lagrangian simulations. It is therefore of high priority to understand what is causing these differences, both in order to be able to perform accurate simulations, as well as to be able to correctly assess the value of the different sub-models available. It is also generally desired to perform as fast calculations as possible, reducing the level of complexity to a minimum without affecting the quality of the predictions.

5.1. The Lagrangian force balance

It has been shown that it is justified to neglect the lift and rotational forces, as well as the thermophoretic force, in simulations

of the urea-SCR system. Although it may look as if the history force could be of some importance at times, this is most probably an erroneous conclusion. Since the history force will always be acting in the same direction as the drag force, the relative influence of the two forces can easily be compared. The integrated effect is in this case approximately two orders of magnitude smaller, and thus history effects may be neglected. It may in fact be more open for discussion whether lift force effects will have a negligible influence, as they will always act in a plane perpendicular to the drag force, and thus a direct comparison is more difficult. In this case the lift force was deemed negligible because of its very low relative importance in terms of integrated transferred momentum.

If stochastic tracking is turned on, the droplets will continuously accelerate and decelerate due to the simulated interaction with turbulent eddies. The droplets will never fully adapt to the gas flow and history effects will thus become more prominent (as seen in Fig. 12). These effects are however still small when compared to the drag force. Based on this reasoning, it should be acceptable to neglect the history force in the Lagrangian force balance for urea-SCR systems.

5.2. Effects of using a detailed drag model

Performing the high gas flow simulations with a detailed drag law instead of a spherical drag law will decrease the overall predicted wall hit with 42% (compare cases 1 and 2 in Fig. 5). The effect is even stronger for the extreme gas flow cases (cases 9 and 10), but the overall wall hit is very low already to start with. The explanation for this decrease lies in the fact that the detailed drag law will, as it takes into account the fact that the droplets will be distorted, predict higher drag coefficients and thus speed up the droplets' adaptation to the gas flow velocity. This will allow the gas to drag away more droplets, and will thus decrease the number of droplets that hit the wall on the opposite side of the injector, which is the large group of droplets hitting the wall.

For the low gas flow simulations, the changes in results are very small when using the detailed drag law instead of the spherical drag law. This is mainly due to the fact that the droplets are much less distorted in the lower gas flow.

5.3. Effects of using a model for stochastic tracking

Using a model for stochastic tracking (i.e. the DRW model) will increase the predicted wall hit in the high gas flow simulations with 76% and in the extreme gas flow simulations with 165%. It is also apparent (from Figs. 5, 8 and 9) that this is in great part due to a phenomenon not seen in the simulations without the DRW model: the collision of droplets with the wall on the injector side of the pipe. This is the part of the pipe where most of the smaller droplets will be present (see Fig. 3). Using the DRW model will thus not only increase the extent of wall hit predicted, but also add new areas for wall hit, as well as new droplet types (i.e. droplets that have lost all their water and are pure urea particles), which were not earlier predicted to hit the wall in the base case simulation.

It can be seen (Table 7) that the decomposition efficiency seen in the simulations is decreased for the high gas flow simulations when using the DRW model. This is mainly caused by the wall boundary condition for droplets, which removes droplets that reach the pipe walls from the simulation. Increased wall hit is thus related to a decrease in decomposition efficiency, which is also the main explanation for the low overall decomposition efficiencies seen in this study. However, the differences in wall hit within the pairs of high gas flow simulation cases with and without the DRW model (i.e. cases 1–2 and 3–4) do not reflect in different decomposition efficiencies, since the differences in wall hit stem from large AdBlue droplets opposite the injector which do not have time to decompose within the pipe anyway, irrespective of whether they reach the wall or not. It is likely that these droplets, if forming an AdBlue film on the wall, would contribute to higher decomposition efficiencies than predicted in these simulations.

It can also be seen from Table 7 that the decomposition efficiency is increased for the low gas flow simulations when using the DRW model. This effect is attributed to that the rates of heat and mass transfer, which will determine the decomposition process, are taken from Nusselt and Sherwood number correlations which are dependent on the droplet Reynolds number. The lowest heat and mass transfer rates will then be predicted for droplets that have been accelerated to the gas velocity without using the DRW model. If the droplets are simulated to interact with turbulent eddies, which will accelerate and decelerate the droplet continuously, the correlations will predict higher rates and thus an increased decomposition efficiency. This is illustrated in Fig. 14, where the relative velocity of a 5 μm droplet is given for simulations of its entire lifetime within the exhaust pipe both with and without the DRW model. Both the higher relative velocities and the shorter lifetime for a droplet simulated with the DRW model are clearly visible. It is of great interest to note that since the correlations used for heat and mass transfer are affected by the use of the DRW model, this will most probably resolve some of the effect of turbulent droplet dispersion on heat and mass transfer that actually takes place within the system. The part that will not be resolved, however, is the part that

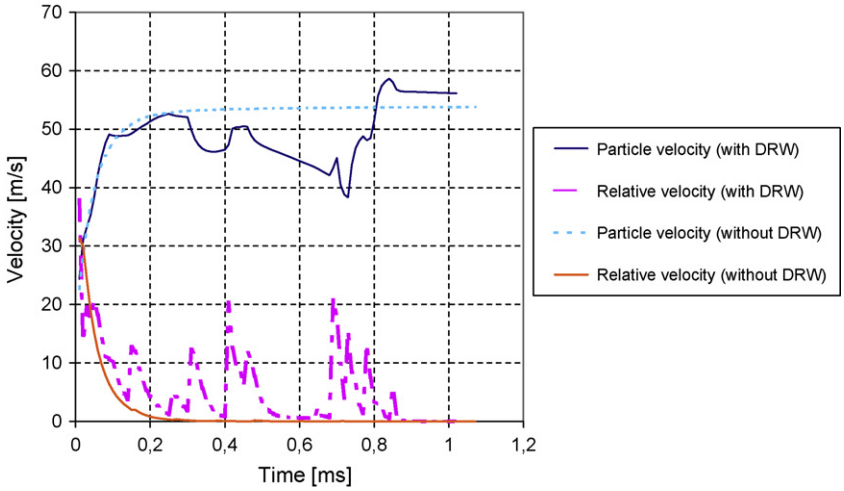

Fig. 14. Droplet velocity and relative velocity between droplet and gas for a 5 μm droplet in high gas flow with and without stochastic tracking. Both simulations have used the detailed drag coefficient.

stems from the acceleration/deceleration taking place in changing directions, which will influence the rearrangement of the boundary layer—something not included in the steady state heat and mass transfer correlations used. For the high and extreme gas flows, the shorter retention time in the pipe and the effects of wall hit on the injector side overshadows these heat and mass transfer effects.

Because of the sensitivity to whether stochastic tracking is used or not, it is of interest to estimate the correctness in the predictions of the DRW model. It is the changes to the droplet velocity in the plane perpendicular to the main gas flow direction (i.e. in the wall-normal directions) that will increase the risk of wall hit in the upper part of the pipe. In the RNG k–ε model, all coordinate directions are equal since the turbulence is assumed to be isotropic. The assumption of isotropy in fully turbulent pipe flow is however not correct, as the magnitude of the fluctuating velocity components will be different in the streamwise direction from the perpendicular directions [45]. Other geometries (bends, branches, diffusers, etc.) will also exhibit similar or even more pronounced deviations from the isotropic turbulence assumption. Great care should thus be taken when deciding on what turbulence model to use in order not to confuse the results when it comes to droplet motion in the gas phase if simulating using a stochastic tracking method. The understanding of the inherent limitations of the turbulence model of choice is thus a crucial modeling component.

The main conclusion must be that the DRW model is sensitive to the quality of the prediction of the turbulent velocity fluctuation by the turbulence model used, and that its inclusion therefore should be carefully evaluated for each new flow situation simulated.

5.4. Wall-film modeling

It was found that the balance between the number of droplets below and above the critical K (40–45) was changed in the different simulation cases, especially for the high gas flow cases. Modeling choices for droplet motion in the gas phase will thus affect not only how many droplets that reach the wall, but also the types of collisions and the cooling effect on the wall. It is therefore very probable that the predictions of a spray/wall-interaction model will also be affected by these modeling choices.

6. Conclusions

The aim of the presented work has been to assess the fidelity and influence of the most commonly used models for Eulerian–Lagrangian CFD-simulations of urea-SCR systems. It has been shown that:

- Modeling choices may affect the predicted extent of wall hit, which types of droplets that are predicted to hit the wall, and also most possibly the simulated effects of wall-wetting if a spray/wall-interaction model is to be included in the simulations.
- In Eulerian–Lagrangian modeling of the urea-SCR system, the drag force and the buoyancy force are enough to correctly describe droplet motion. If submicron-scale behavior is to be resolved, Brownian motion must be modeled and the Cunningham drag correction must be employed.
- The distortion of the droplets will affect their drag coefficients, which can be accounted for through the use of a dynamic particle drag law, where the current level of droplet distortion is taken into account. As the simulation results will depend on the predicted momentum transfer from the gas to the droplets, this must be accurately modeled. The larger the droplets are, the more pronounced the distortion effects will become.
- Turbulent effects on droplet trajectories are large enough to require modeling. Inclusion of a stochastic model such as the DRW model will help describe these turbulent effects, but also makes the simulation results sensitive to the quality of the turbulence model's prediction of the turbulent fluctuating velocities. It might very well be necessary to employ a more advanced turbulence model than a k–ε variant, depending on the geometry of the system. Using the DRW model will also help resolve some of the enhancement of heat and mass transfer due to the continuous acceleration/deceleration of droplets by the interaction with turbulent eddies.

Acknowledgements

This work has been performed within the Competence Centre for Catalysis, which is financially supported by Chalmers University of Technology, the Swedish Energy Agency and the member companies: AB Volvo, Volvo Car Corporation, Scania CV AB, GM Powertrain Sweden AB, Haldor Topsoe A/S and The Swedish Space Agency.

Thanks also to Linda Hellström for helping out with the graphics.

References

[1] M. Koebel, M. Elsener, M. Kleemann, Urea-SCR: a promising technique to reduce NOx emissions from automotive diesel engines, Catal. Today 59 (2000) 335–345.
[2] J.N. Chi, H.F.M. DaCosta, Modeling and control of a urea-SCR aftertreatment system, SAE Technical Paper (2005) 2005-01-0966.
[3] M. Chen, S. Williams, Modelling and optimization of SCR-exhaust aftertreatment systems. SAE Technical Paper (2005) 2005-01-0969.
[4] N.A. Chigier, The Physics of Atomization, in: Proceedings of the 5th International Conference on Liquid Atomization and Spray Systems (ICLASS-91), National Institute of Standards and Technology, 1991.
[5] M. Koebel, M. Elsener, G. Madia, Recent advances in the development of urea-SCR for automotive applications, SAE Technical Paper (2001) 2001-01-3625.
[6] D.R. Linde (ed.), CRC Handbook of Chemistry and Physics, Internet Version 2007, 87th ed., Taylor & Francis, Boca Rato, FL, 2007.
[7] T.Y. Oh, J.H. Ko, H.J. Seong, B.S. Min, Design optimization of the mixing chamber in SCR system for marine diesel engine, in: Proceedings of the 6th International Symposium on Diagnostics and Modeling of Combustion in Internal Combustion Engines, vol. 6, The Japan Society of Mechanical Engineers, 2004, pp. 87–92.
[8] W.H. Sun, J.M. Boyle, P.G. Carmignani, J.M. Sassenrath, Small scale test results from new selective catalytic NOx reduction process using urea, in: Proceedings of the MEGA Symposium, Chicago, IL, 2001.
[9] P.M. Schaber, J. Colson, S. Higgins, D. Thielen, B. Anspach, J. Brauer, Thermal decomposition (pyrolysis) of urea in an open reaction vessel, Thermochim. Acta 424 (2004) 131–142.
[10] L. Stradella, M. Argentero, A study of the thermal decomposition of urea, of related compounds and thiourea using DSC and TG-EGA, Thermochim. Acta 219 (1993) 315–323.
[11] J.L. Calabrese, J.A. Patchett, K. Grimston, G.W. Rice, G.W. Davis, The influence of injector operating conditions on the performance of a urea–water selective catalytic reduction (SCR) system, SAE Technical Paper (2000) 2000-01-2814.
[12] S. Sluder, J. Storey, S. Lewis, L. Lewis, Urea decomposition and SCR performance at low temperature, in: Proceedings of the 10th Annual DEER Workshop, Coronado, CA, 2004.
[13] F. Birkhold, U. Meingast, P. Wassermann, O. Deutschmann, Analysis of the injection of urea–water-solution for automotive SCR DeNOx-systems: modeling of two-phase flow and spray/wall interaction, SAE Technical Paper (2006) 2006-01-0643.
[14] F. Birkhold, U. Meingast, P. Wassermann, O. Deutschmann, Modeling and simulation of the injection of urea-water-solution for automotive SCR DeNOx-systems, Appl. Catal. B 70 (2007) 119–127.
[15] H.L. Fang, H.F.M. DaCosta, Urea thermolysis and NOx reduction with and without SCR catalysts, Appl. Catal. B 46 (2003) 17–34.
[16] C.S. Sluder, J.M.E. Storey, S.A. Lewis, L.A. Lewis, Low-temperature urea decomposition and SCR performance, SAE Technical Paper (2005) 2005-01-1858.
[17] M. Koebel, G. Madia, M. Elsener, Selective catalytic reduction of NO and NO_2 at low temperatures, Catal. Today 73 (2002) 239–247.
[18] J.C. Ball, A toxicological evaluation of potential thermal degradation products of urea, SAE Technical Paper (2001) 2001-01-3621.
[19] G. Stiesch, Modelling Engine Spray and Combustion Processes, Springer–Verlag, Berlin, 2003.
[20] Fluent, Inc., Fluent 6.3 Documentation, 2007.
[21] F. Ekström, B. Andersson, Pressure drop of monolithic catalytic converters—experiments and modeling, SAE Technical Paper (2002) 2002-01-1010.
[22] R.D. Reitz, C.J. Rutland, Development and testing of diesel engine CFD models, Prog. Energy Combust. Sci. 21 (1995) 173–196.
[23] B. Andersson, R. Andersson, L. Håkansson, M. Mortensen, R. Sudiyo, B. van Wachem, Computational Fluid Dynamics for Chemical Engineers, Chalmers University of Technology, Gothenburg, 2008.
[24] C.N. Davies, Definitive equations for the fluid resistance of spheres, Proc. Phys. Soc. 57 (4) (1945) 259–270.

[25] R. Clift, J.R. Grace, M.E. Weber, Bubbles, Drops and Particles, Academic Press, New York, 1978.
[26] M.C. Yuen, L.W. Chen, On drag of evaporating liquid droplets, Comb. Sci. Technol. 14 (1976) 147–154.
[27] B.T. Helenbrook, C.F. Edwards, Quasi-steady deformation and drag of uncontaminated liquid drops, Int. J. Multiphase Flow 28 (2002) 1631–1657.
[28] N.I. Kolev, Multiphase Flow Dynamics 2. Thermal and Mechanical Interactions, Springer–Verlag, Berlin, 2005.
[29] R.J. Haywood, M. Renksizbulut, G.D. Raithby, Numerical solution of deforming evaporating droplets at intermediate Reynolds numbers, Numer. Heat Transfer: Part A 26 (1994) 253–272.
[30] C. Crowe, M. Sommerfeld, Y. Tsuji, Multihpase Flows with Droplets and Particles, CRC Press, Florida, 1998.
[31] W.D. Warnica, M. Renksizbulut, A.B. Strong, Drag coefficients of spherical liquid droplets. Part 2. Turbulent gaseous fields, Exp. Fluids 18 (1995) 265–276.
[32] P.H.T. Uhlherr, C.G. Sinclair, The effect of free-stream turbulence on the drag coefficient of sphere, in: A Conference Convened by the Australian National Committee of the Institution of Chemical Engineers and the Australian Academy of Science (Chemeca-70), Chatswood, Australia, 1970.
[33] T.J. Anderson, P.H.T. Uhlherr, The influence of stream turbulence on the drag coefficient of freely entrained spheres, in: Preprints of Papers to the Sixth Australasian Hydraulics and Fluid Mechanics Conference, 1977, pp. 541–545.
[34] D. Petrak, Drag force of freely moving single and cloud spheres in case of counter-current turbulent gas–solid flow, Chemische Technik 28 (1976) 591–595.
[35] R. Kurose, S. Komori, Drag and lift forces on a rotating sphere in a linear shear flow, J. Fluid Mech. 384 (1999) 183–206.
[36] L.-S. Fan, C. Zhu, Principles of Gas–solid Flows, Cambridge University Press, Cambridge, 1998.
[37] L. Talbot, R.K. Cheng, R.W. Schefer, D.R. Willis, Thermophoresis of particles in a heated boundary layer, J. Fluid Mech. 101 (1980) 737–758.
[38] F. Odar, W.S. Hamilton, Forces on a sphere accelerating in a viscous fluid, J. Fluid Mech. 18 (1964) 302–314.
[39] N. Frössling, On the evaporation of falling drops, Gerl. Beitr. Zur Geophysik 52 (1938) 170–216.
[40] D.I. Kolaitis, M.A. Founti, A comparative study of numerical models for Eulerian–Lagrangian simulations of turbulent evaporating sprays, Int. J. Heat Fluid Flow 27 (2006) 424–435.
[41] R.C. Reid, J.M. Prausnitz, T.K. Sherwood, The Properties of Gases and Liquids, third ed., McGraw-Hill Book Company, 1977.
[42] E.M. Sparrow, J.L. Gregg, The variable fluid-property problem in free convection, Trans. ASME 80 (1958) 879–886.
[43] Spray/Wall-Interaction Modelling by Dimensionless Data Analysis, PhD Thesis, Shaker Verlag, Aachen, 2004.
[44] E.P. Perman, T. Lovett, Vapour pressure and heat of dilution of aqueous solutions, Trans. Faraday Soc. 22 (1926) 1–19.
[45] J.G. Eggels, F. Unger, M.H. Weiss, J. Westerweel, R.J. Adrian, R. Friedrich, F.T.M. Nieuwstadt, Fully developed turbulent pipe flow: a comparison between direct numerical simulation and experiment, J. Fluid Mech. 268 (1994) 175–209.
[46] A.A. Kozyro, S.V. Dalidovich, A.P. Krasulin, Heat capacity, enthalpy of fusion, and thermodynamic properties of urea, Zh. Prikl. Khim. (Leningrad) 59 (7) (1986) 1456–1459.
[47] G. Hellsten, Tabeller och Diagram, 1st ed., Almqvist och Wiksell Förlag AB, 1992.